5-22-2020

Projections of Change in Frequency and Persistence in Atmospheric Ridging Over the Pacific Northwest Using CMIP6 Models

Ellen Koukel
Portland State University

Projections of Change in Frequency and Persistence in Atmospheric Ridging over the Pacific Northwest using CMIP6 Models

by

Ellen Koukel

An undergraduate honors thesis submitted in partial fulfillment of the

requirements for the degree of

Bachelor of Science

in

University Honors

and

Environmental Physics

Thesis Advisor

Paul Loikith, Ph.D.

Portland State University

2020

I. INTRODUCTION

Atmospheric ridging events can be defined as broad and persistent positive geopotential height anomalies over a region, often defined at 500 hPa, hereafter Z500 (Gibson et al. 2020; Liu et al. 2018; Swain et al. 2017). Geopotential height is the altitude of a pressure surface above mean sea level. Higher pressure surfaces are indicative of a ridge and often prevent the storm track from passing through, forcing it poleward. Ridges are also characterized by the northward displacement of the jet stream around an area of high pressure.

The effect of climate change on ridging in the Pacific Northwest has had little research, but a far more robust area of research focuses on blocking events worldwide. Blocking events are large atmospheric features linked to regions of high pressure, and are alternatively defined as stationary ridges in a large amplitude Rossby wave (Woollings et al. 2018; Parsons et al. 2016). Blocking events can be considered ridges with slow phase speed; ridges that are not blocking events progress with a faster phase speed. Thus, as the basic tenets of blocking events are persistent positive anomalies and are therefore slower ridges (Renwick 2005), one can apply research on blocking events to ridges, as has been done by Gibson et al. (2020)

Atmospheric ridging significantly affects the weather of the area that it influences, which is often directly underneath (Davini et al. 2012). Persistent ridging often leads to extended periods of anomalously warm and dry weather and can lead to prolonged droughts and heatwaves (Parsons et al. 2016; Liu et al. 2018; Peng et al. 2019; Teng and Branstator 2017; Brewer and Mass 2016; Gibson et al. 2020). One extreme example of this was the severe drought and anomalous warmth in California of winter 2013-2014, caused almost exclusively by a persistent ridge off the West Coast (Peng et al. 2019; Wang et al. 2014; Teng and Branstator 2017; Mundhenk et al. 2016; Swain et al. 2017). This was nicknamed the "Ridiculously Resilient Ridge" due to its sheer persistency that diverted precipitation and storms northward (Swain 2015). The severity of the drought was compounded by climate change; ridges are warmer and their effects are exacerbated by a changing climate, as the severity of the Ridiculously Resilient Ridge was far worse than if it had happened pre-1960. Significantly, the Ridiculously Resilient Ridge blocked atmospheric rivers, which bring large amounts of precipitation to both California and the Pacific Northwest. When ridges are present, extra-tropical cyclones and atmospheric rivers are deflected northward, sending precipitation away from the ridge (Mundhenk et al. 2016; Parsons et al. 2016). Persistent positive Z500 anomalies, such as ridging, indicate a warmer than average atmospheric column as well as reduced relative humidity and precipitation, meaning a warmer and drier area under a ridge (Röthlisberger et al. 2016). Additionally, ridges, through prevention of storm track permeation and subsidence, mean clearer skies, which results in enhanced solar heating and warmer-than-average daily temperatures (Brewer and Mass 2016).

As climate change continues worldwide, the Arctic is warming at a faster rate – almost twice as quickly – as the rest of the world (Francis and Vavrus 2012). This phenomenon, termed Arctic amplification (AA), has been hypothesized as responsible for many of the changes in weather patterns in the northern mid-latitudes, such as increased extreme droughts or precipitation (Francis and Vavrus 2012; Francis and Skific 2015). It is proposed that AA causes an increase in jet stream meridional character, or north-south waviness (Francis and Skific 2015), due to a lowering of temperature contrast between the Arctic and mid-latitudes. The temperature contrast is a significant driver of the jet stream's westerly, or zonal, wind speeds, so a lower ratio of high latitude to mid latitude temperatures would reduce the zonal wind (Francis and Skific 2015) in 1000 - 500 mb height layer (Francis and Vavrus 2012). While the jet stream slows zonally, enhanced high-latitude warming causes Z500 heights to rise higher than Z500 heights in

the mid-latitudes, thus potentially elongating ridges northward, slowing their phase speed, and increasing jet stream wave amplitude (Francis and Vavrus 2012; Francis and Skific 2015). According to Francis and Vavrus (2012) and Francis and Skific (2015), then, slower zonal winds combined with a wavier stream increase the possibility of persistent northern mid-latitude weather patterns that cause extreme weather events. Additionally, AA and the associated effects may include an increase in long-duration events, defined by Francis et al. (2018) as weather events lasting four or more consecutive days (2018). Therefore, one could expect potential weather patterns to contain more persistent extremes (Francis and Vavrus 2012; Francis and Skific 2015; Francis et al. 2018), such as drought, floods, cold and heat waves (Francis and Vavrus 2012), and storminess (Francis et al. 2018) due to AA. Röthlisberger et al. (2016) describes how jet stream waviness is a primary driver of daily weather extremes in northern mid-latitudes. They note that regional jet stream waviness is more important to weather extremes than hemisphere-wide jet stream waviness. Thus, regional changes in the waviness of the jet stream due to climate change are important to changing wind, precipitation, and temperature extremes, as well as atmospheric ridging. (Rothlisberger et al. 2016)

However, Barnes (2013) and Screen and Simmonds (2013) counter the previous point of AA causing an increase in jet stream waviness. In an analysis done by Barnes (2013), there is no zonal slowing of the jet stream except in October-November-December, and that is due to analysis parameters. When a shift in geopotential height is accounted for, unlike in previous scholarship, there is no significant change in wave amplification, as well as no increase in the existence of atmospheric ridges. Thus, as there is no increase in atmospheric ridge occurrence, as well as no trends of decreasing zonal speeds or increasing meridional character, they write that AA is not the sole cause of changing mid-latitude weather patterns, nor altering the amplitude or phase speed of atmospheric ridges (Barnes 2013). Screen and Simmonds (2013) add that connections between AA and the jet stream, and therefore mid-latitude weather patterns, are sensitive to the conceptualization of planetary waves. Therefore, both zonal and meridional speeds and amplitudes have complex ramifications for mid-latitude weather trends (Screen and Simmonds 2013). Thus, while AA and jet stream waviness are proposed to be responsible for changes in atmospheric ridging and mid-latitude weather, there is not just one cause.

Another explanation for the presence and persistence of atmospheric ridging in the Pacific Northwest lies in North Pacific Ocean sea surface temperature (SST). Bond and Harrison (2000) write that mid-latitude atmospheric events, such as ridges, are strongly affected by SST. SST may actually create and maintain atmospheric ridges, rather than atmospheric circulation patterns determining SST. The Pacific Decadal Oscillation (PDO) affects North Pacific SST, with warmer SST during a positive PDO phase and cooler SST during a negative PDO phase. When the PDO is in a positive phase, there are more atmospheric troughs, and when the PDO is in a negative phase, there are more atmospheric ridges over the North Pacific and western North America. Thus, propose Bond and Harrison, both SST and therefore atmospheric ridging are affected by the PDO. (Bond and Harrison 2000) Yet during the winter of 2013-2014, the Pacific Ocean was in a neutral ENSO phase and the PDO was not strong (Teng and Branstator 2017; Wang et al. 2014). However, this does not mean that neither ENSO nor PDO affect atmospheric ridging – merely, they were not primary causes of one significant ridging event in recent history. Seager et al. (2015), and later Seager and Henderson (2016), write that SST is key to sustaining atmospheric ridging. While SST was integral to the persistence and existence of the 2013-2014 winter California ridge, it was limited to one-third to one-half of the supplying forcing. Swain et al. (2017) as well discuss how SST may cause persistence of atmospheric ridging. In the future,

SST will increase due to global warming, potentially affecting atmospheric wave patterns. Understanding the effect of SST, as well as other factors on atmospheric ridging, will likely be important in understanding future atmospheric ridging and related weather patterns (Swain et al. 2017).

As global warming progresses and the earth's climate continues to change, researchers need to create a thorough understanding of atmospheric dynamics. AA and SST are both likely to change drastically in the future, as both the Arctic and the oceans will continue to warm due to anthropogenic forcing (Wang et al. 2014; Woollings et al. 2018). Hoskins and Woollings (2015) state the need to understand what we can expect in the future, as greenhouse gas concentrations continue to rise. Woollings et al. (2018) provide a solid overview of the troubles associated with researching persistent positive anomalies and the effects climate change will have on such events, including ridging. Some difficulties include differences in persistent positive anomaly measurements, such as absolute versus departure fields, as well as past climate models continually underestimating ridging. However, they do hypothesize that although ridging will likely decrease, ridges will continue to be an important source of weather extremes throughout the twenty-first century (Woollings et al. 2018). Changes in either SST or AA are only potential driving mechanisms for changes in atmospheric ridging. This paper aims to investigate potential changes in frequency and persistence of springtime atmospheric ridging in the Pacific Northwest under future climate change.

II. METHODS AND DATA

a. Data

Daily mean geopotential height at 500 hPa data are from ten models from the Coupled Model Intercomparison Project Phase 6 (CMIP6), as seen in Table 1. CMIP6, available publicly online (https://esgf-node.llnl.gov/projects/cmip6/) is the latest iteration of the Coupled Model Intercomparison Project (CMIP), a coordinated climate modeling effort from modeling groups all over the world. The CMIP effort has historically informed the Intergovernmental Panel on Climate Change and is publicly available. All future CMIP6 model data used the SSP585 emission pathway, which uses the greatest amount of greenhouse gas emissions out of all emission scenarios. All models were bilinearly regridded to a 2° latitude x 2° longitude grid mesh. CMIP6 models were used to determine model fidelity to observational data and projections of future ridging characteristics. Z500 data were also taken from a NASA reanalysis product, the Modern-Era Retrospective analysis for Research and Applications, Version 2 (MERRA2), also seen in Table 1. MERRA2 data were used as the observational basis of ridging events and precipitation. Precipitation data were also taken from the Blazed Alder SNOTEL station, located within the Bull Run watershed, as seen in Table 1.

MODEL NAME	RESOLUTION	REFERENCE
BCC-CSM2-MR	1.125° × 1.125°	Xin et al. 2019; Wu et al. 2018
CanESM5	1.875° × 1.875°	Swart et al. 2019
CESM2-WACCM	0.9° × 1.25°	Danabasoglu et al. 2019
GDFL-CM4	1° × 1°	Guo et al. 2018
INM-CM5-0	2° × 1.5°	Volodin et al. 2019
MIROC6	1.39° × 1.39°	Tatebe et al. 2018; Shiogama et al. 2019
MPI-ESM1-2-HR	0.9° × 0.9°	Schupfner et al. 2019; Jungclaus et al. 2019
MRI-ESM2-0	1.125° × 1.125°	Yukimoto et al. 2019
NorESM2-LM	1.9° × 2.5°	Seland et al. 2019
NorESM2-MM	0.9° × 1.25°	Bentsen et al. 2019
MERRA2	0.5° × .625°	Gelaro et al. 2017
Blazed Alder SNOTEL	-	USDA 2019

Table 1. List of ten used CMIP6 models, their native resolution, and reference, as well as resolution and source for MERRA2 and Blazed Alder SNOTEL datasets.

b. Methodology

Daily geopotential height anomalies were constructed from daily geopotential height CMIP6 model data as departures from the long-term 30-year daily mean for the chosen time period. The mean for each day of spring was found using daily geopotential height data from 30 years, creating 92 daily means for the 92 days of meteorological spring. This was subtracted from daily geopotential height data, creating daily geopotential height anomalies for all 92 spring days for all 30 years of the chosen time period. Once the anomalies were detrended and the global warming signal was removed, as outlined below, geopotential height anomalies were normalized. Normalization was done by dividing daily geopotential height anomalies by the standard deviation of daily geopotential height anomalies for all days in the thirty year period that occurred during the month of the original anomaly.

Prior to computing the data used in this paper, the global warming signal was removed from the daily geopotential height model data. The atmosphere will expand as the earth's climate warms, and thus all future geopotential heights will be higher than in the past. Removing the global warming signal enables future Z500 anomalies to be directly compared to the historical anomalies, without having to factor in the additional atmospheric expansion. The global warming signal was computed by subtracting the mean northern hemisphere historical 500 hPa geopotential height from the mean northern hemisphere mid- or late-century 500 hPa geopotential height. The global warming signal was then removed from each Z500 value for the chosen time period. This was done on a model by model basis, where the global warming signal was found for each model and only used with data for that particular climate model.

In order to determine whether or not a ridge was present, an algorithm was developed to process the data. The algorithm is dependent on Z500 anomalies over a chosen geographic area, the cyan box in Figure 1, similar to the persistent positive anomaly approaches taken by Gibson et al. (2020) and Teng and Branstator (2017). For a ridge to occur, at least fifty percent of the box must have Z500 anomalies greater than +0.5 standard deviations and less than twenty-five percent of the area must have Z500 anomalies less than -0.2 standard deviations. The algorithm was perfected using performance metrics outlined by Gao et al. (2017), based on the number of dry and wet days captured.

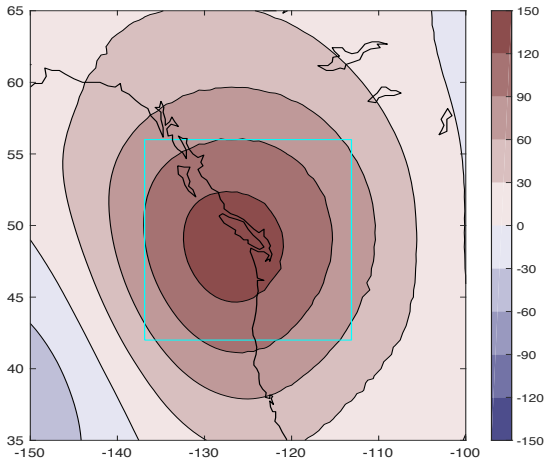

Fig. 1. Map of index region (cyan box), showing average spring ridge day Z500 anomalies for historical MERRA2. Dark reds indicate higher positive geopotential height anomalies and typify a ridge.

Meteorological spring includes the months of March, April, and May which are of considerable importance for Pacific Northwest precipitation. The work done in this paper largely concerns ridging frequency and persistence. Ridge frequency is defined as the number of days when a ridge occurred. Ridge persistence is the length of time that a specific ridge event occurred, with at least one non-ridge day occurring between two ridging events. The historical period is defined as the years 1981-2010, mid-century is 2031-2060, and late-century is 2071-2100. Most of the time ridges are present, there is no precipitation in the area underneath a ridge. Days with precipitation are defined as days with greater than three millimeters of precipitation, to allow for morning dew on the sensors.

III. RESULTS

a. Bull Run Background

This paper focuses on springtime atmospheric ridging over the area surrounding the Bull Run watershed, just east of Portland, Oregon. The Bull Run watershed supplies the majority of the water to the Portland metropolitan area and is a primarily rainfed basin. The hydroclimatology of the Pacific Northwest is characterized by wet winters and dry summers; however, the rainy season is subject to considerable year to year variability. Early onset of the dry season can introduce challenges for water resource managers, as anomalously dry springs are historically due to persistent atmospheric ridging; increased ridging in late spring can prematurely end the rainy season. Notable examples are May 2015 and 2018, as seen in Figures 2a and 2b. Figures 2a and 2b show the Z500 anomalies for all days for the entire month, showcasing an abnormally high amount of ridging for the end of meteorological spring. Figure 2c shows precipitation totals for Mays from 1981-2018 in the Bull Run basin at the Blazed Alder SNOTEL station, highlighting exceedingly low precipitation totals for May 2015 and 2018.

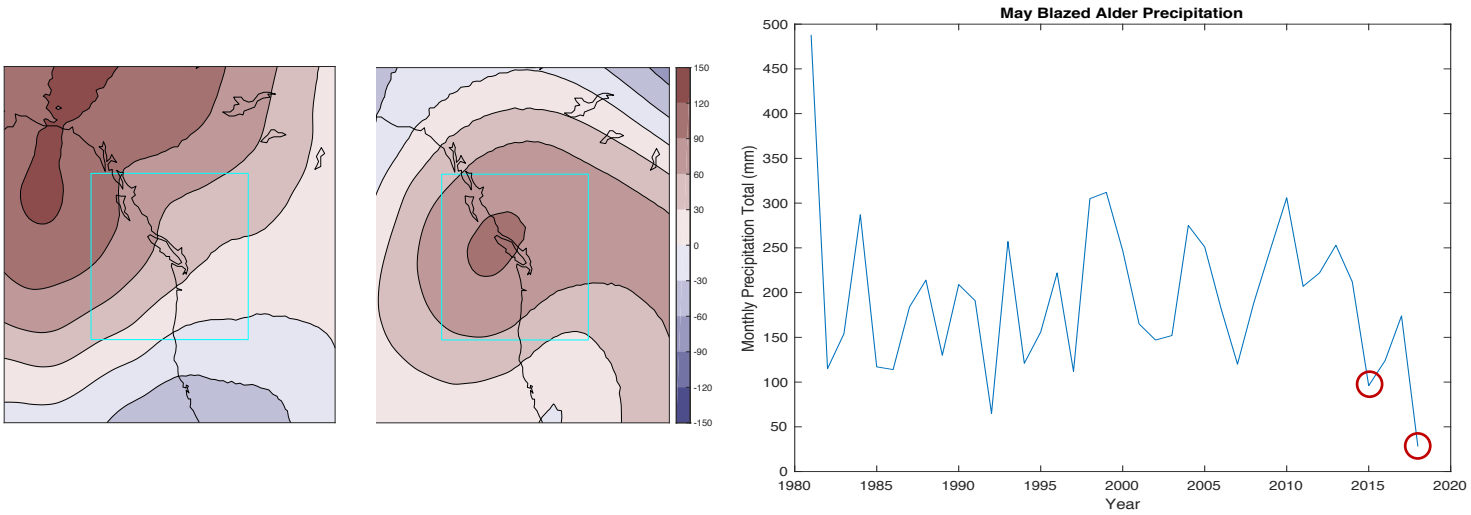

Fig. 2. Map of index region (cyan box), showing (a) average May 2015 Z500 anomalies and (b) average May 2018 Z500 anomalies. Dark reds indicate higher pressure and typify a ridge. (c) shows May precipitation totals by year at the Blazed Alder SNOTEL station near the Bull Run basin, with 2015 and 2018 circled in red.

b. Climatology

The climatology of the region surrounding the Bull Run watershed was created using Z500 data from MERRA2 and precipitation data from the Blazed Alder SNOTEL station. Figure 3a shows that monthly precipitation is generally inversely proportional to the number of ridges during that month. There are a few notable examples of this. 2015 and 2018, as discussed in Section IIIa, Figure 2, show substantial amounts of ridging during the month of May, and correspondingly very little rainfall. Other examples are 2004 and 1990, where there is significant ridging throughout spring, particularly March and April for both years. March and April 1990 and 2004 had very few days with precipitation. 1992 was also a very dry year, as March and May had lots of ridging with little rainfall. The opposite pattern also exists; there are many years with very little ridging and many days of precipitation. One such year is 2011, where no ridges occur in March and April. As expected, there were many wet days in 2011, likely due to there only being three ridge days that entire spring. This pattern occurs again in 2003, as there were no ridges in April of that year and many days with precipitation in April 2003. March and May of 2003 were also considerably rainy, as there was very little ridging throughout those months.

Figure 3b shows ridge days, the center of the largest ridge of the year, and precipitation. Ridge days are denoted by blue circles, and precipitation by the presence of a green dot, with a larger green dot indicating higher rainfall. The center of the longest ridge is shown by a red 'X.' In the last decade, there has been a tendency towards the longest ridge of spring occurring in late May, as seen by the gathering of red 'X's beginning roughly in 2006. There is no discernable pattern for the years before then. Again, May 2015 and 2018 stand out in this figure. Both 2015 and 2018 have the middle of the largest ridge occurring in late May. Additionally, both have very few ridge days that coincide with precipitation. When there is precipitation on a ridge day, it is a very small amount, as shown by a small green dot inside a blue circle. Other years are of interest as well. 1990, already described from Figure 3a, has a very long stretch of ridging through March and April, broken up by two days that are not ridges but had no precipitation. 1990 had very little precipitation in spring, with only one day of heavy rainfall occurring in late March. 1981 and 1993 were very wet years. Many of the days in 1981 and 1993 have green dots, many of them large, indicating heavy precipitation.

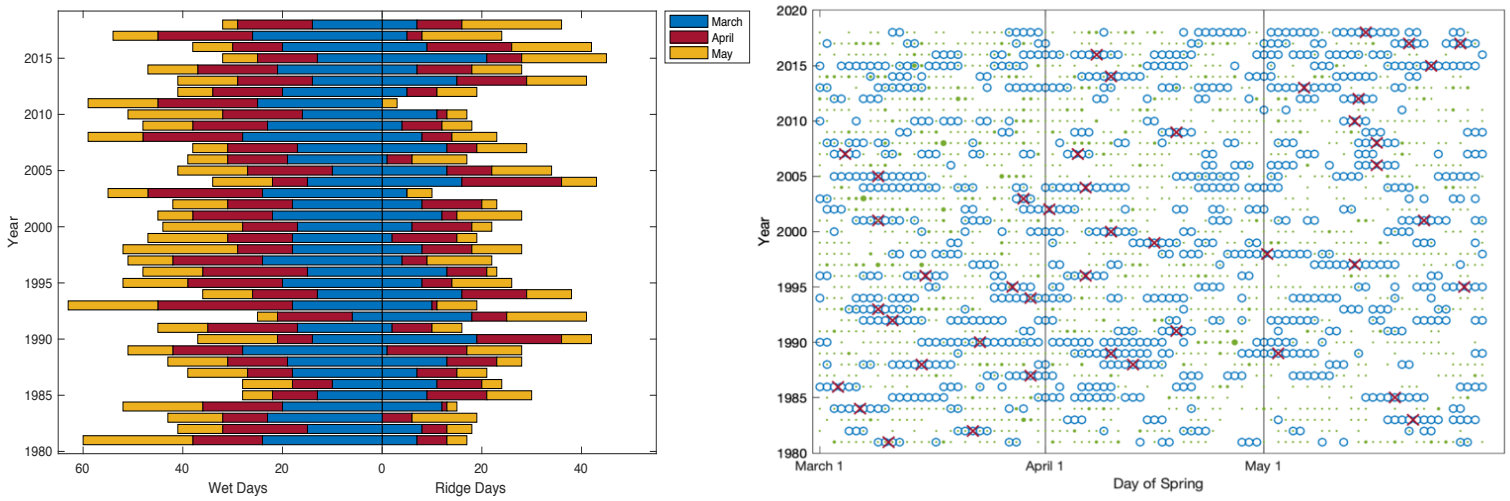

Fig. 3. Climatology of the region surrounding the Bull Run watershed. (a) Observed number of ridge days on the right, starting from center, compared to number of days where precipitation occurred on the left, starting from center, in the Bull Run watershed east of Portland, Oregon. The month of March is blue, the month of April is red, and the month of May is gold. (b) Observed climatology of ridges and precipitation. Blue circles denote days with a ridge, red 'X's denote middle of longest ridge event that spring, and green dots denote days with precipitation, with size of dot increasing as precipitation increases.

c. Model Evaluation

CMIP6 historical models capture ridge climatology with reasonable skill. Figure 4 shows average ridge day Z500 composite maps for historical simulations from all 10 models, with darker red indicating higher geopotential heights. This was done in order to determine whether the historical models accurately depict ridging. All models show ridging as expected through the historical period, thus boosting confidence in future projection credibility. All are comparable to observational reanalysis data of the region, shown in Figure 1 above, which shows promise for the capabilities of the models in accurately resolving 500 hPa geopotential height. A few of the models are notable. BCC-CSM2-MR, for example, produces generally larger ridges with bigger

magnitudes than the other models. In contrast, INM-CM5-0 produces smaller ridges with short magnitudes. The other eight models fall in between those two.

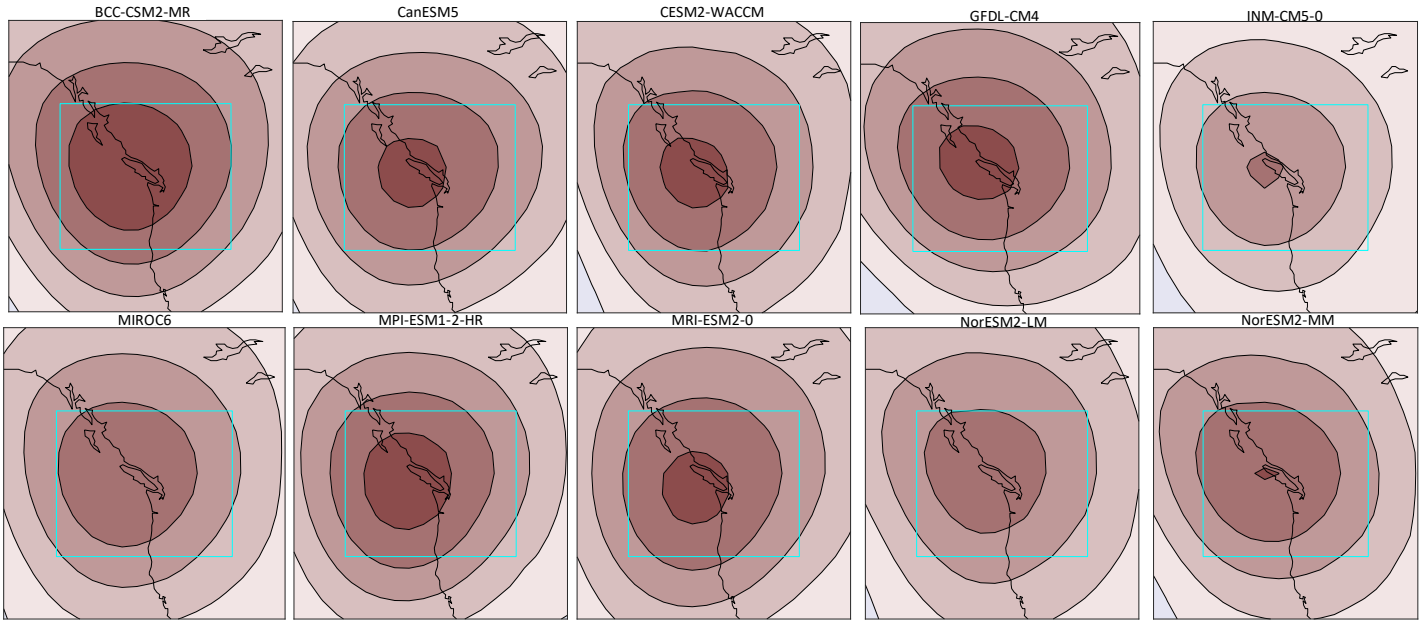

Fig. 4. Average ridge day Z500 composite maps for ten historical models. Darker reds indicate higher anomalies and thus a ridge. Index region is defined by cyan box.

Figure 5 shows CMIP6 model evaluation, with a comparison of historical model ridge persistence and frequency to the MERRA2 reanalysis. Ridge length in the historical period, as seen in Figure 5a, is slightly oversimulated, with 7 of the ten models having a median ridge length of 3 days, while MERRA2 and the remaining three models – CanESM5, INM-CM5-0, and MPI-ESM1-2-HR – provide a median ridge length of 2. No statistical significance tests have been applied and thus there is no quantitative certainty on model performance. However, results suggest reasonable agreement.

The number of ridge days, as seen in Figure 5b, is also oversimulated in the models. MERRA2 gives a median of 23 as the number of ridge days in a spring and is matched by only one model, GFDL-CM4. No models undersimulate the number of ridge days in a year. Nine of the models oversimulate the median number of ridge days in a year by 2 to 6 days. Two models, CanESM5 and CESM2-WACCM, have the same highest outlier as MERRA2, while three models – BCC-CSM2-MR, GFDL-CM4, and NorESM2-MM – have an outlier of up to five more days of ridging in a single year. Five models – INM-CM5-0, MIROC6, MPI-ESM1-2-HR, MRI-ESM2-LM, and NorESM2-LM – have a smaller highest outlier than MERRA2. While the frequency of ridging is slightly oversimulated, the models have an accurate grasp of atmospheric patterns that define ridging events. Due to the method used to define ridging based on standardized anomalies, it is expected for the model data to show a similar number of simulated ridges as the observational reanalysis. This is useful, however, as it shows that the models well capture the mechanisms behind atmospheric ridging that is analogous to the real world.

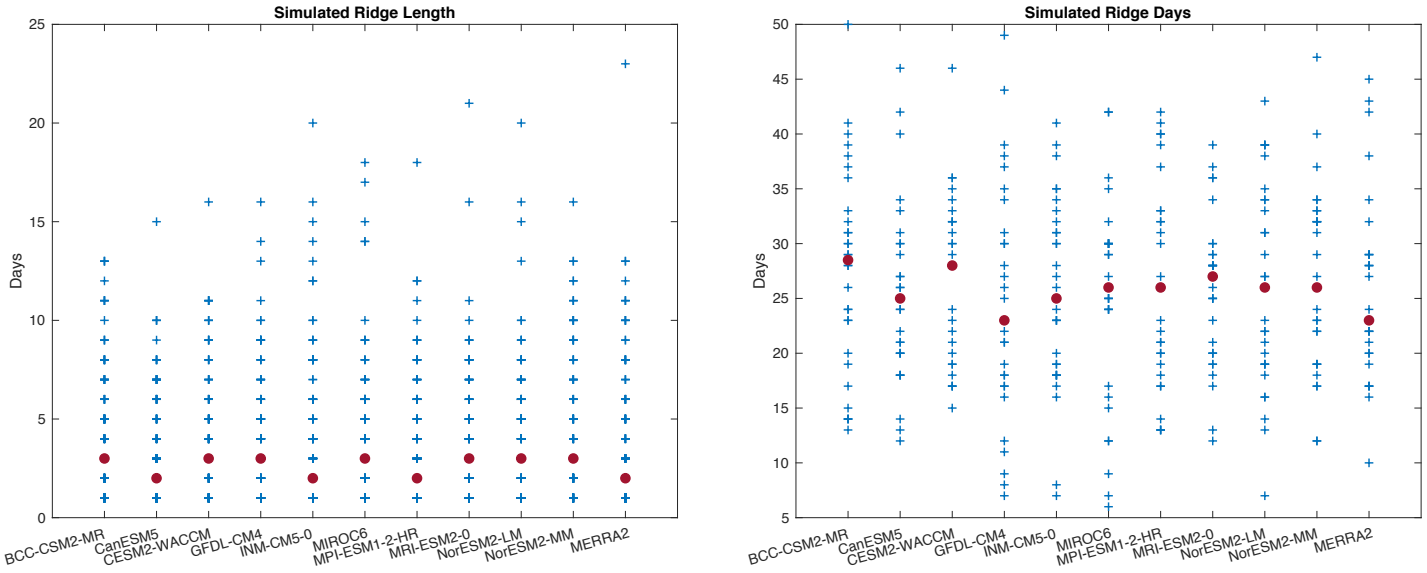

Fig. 5. Simulated ridge (a) persistency and (b) frequency of ten CMIP6 models, compared against MERRA2 reanalysis data (far right).

d. Future Projection

Figure 6 shows CMIP6 model projections, comparing the historical period to the mid- and late-century, for both frequency and persistence. The median length of a simulated ridge event as seen in Figure 6a remains the same across all time periods when all models are considered together, with the median length being 3 days. The largest outliers, however, decrease in size over time. The largest outlier in the historical period is a ridge lasting 28 days, while the largest outlying ridge in the mid-century lasts 24 days, and the longest ridge lasts only 21 days in the late-century. A majority of the models, when considered individually, experienced a slight decrease over time in the length of ridging events.

The number of ridge days per spring, as seen in Figure 6b when all ten models are considered together, increases from 25 to 26 from the historical to the mid-century. The late-century median remains 26. The largest outlier in the historical period is 55 ridge days per spring, decreasing to the single outlier of 51 for mid-century. There are no outliers for the late-century period.

Overall, ridge persistence and frequency decrease very slightly from the historical to the mid-century, and evens out as it approaches late-century. There are no substantial changes in either persistence or frequency. No statistical significance tests have been applied and therefore there is no quantitative significance of the decrease in ridge frequency and persistency.

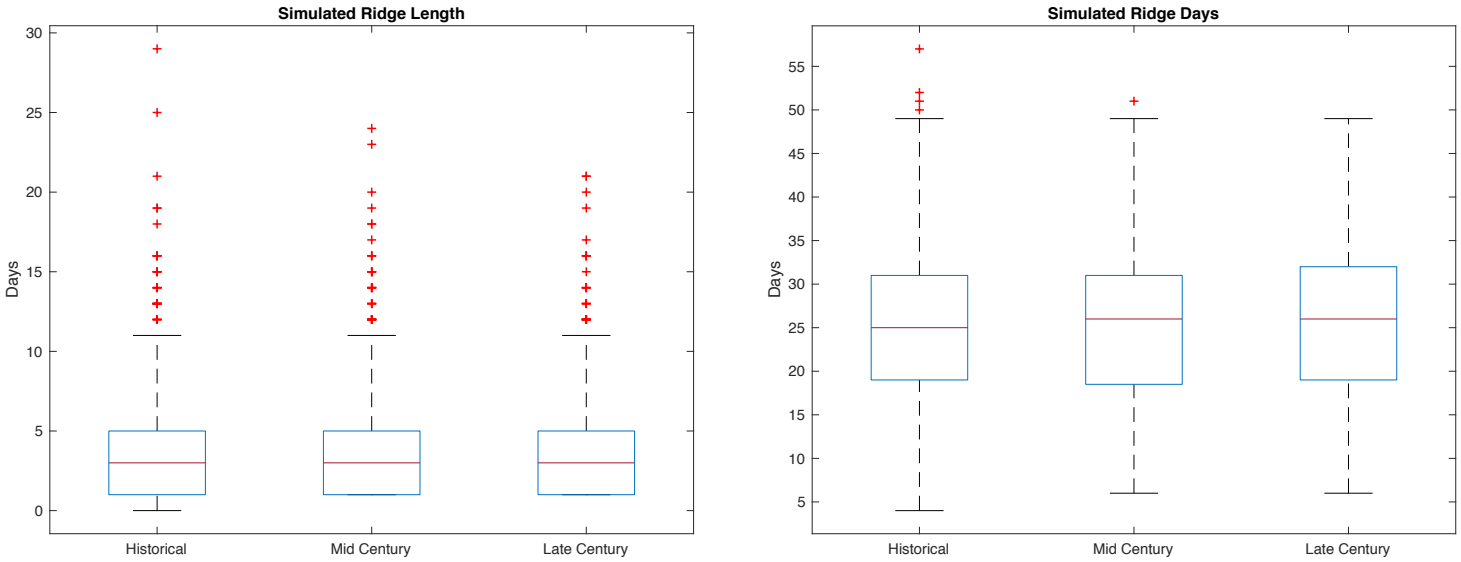

Fig. 6. Simulated ridge (a) persistency and (b) frequency for a combined ten models, showing historical, mid-century, and late-century ridging simulations. The red lines in the middle of the blue boxes represent the median of the data. The blue boxes represent the middle fifty percent of the data and the black whiskers extend to the fifth and ninety-fifth percent of the data. The red outliers are data above the ninety-fifth percent, as no outliers exist in the bottom five percent.

IV. CONCLUSION

The climate models looked at here generally capture ridging climatology with reasonable fidelity. While the climate models looked at in this study do not perfectly match MERRA2 observational reanalysis, they perform adequately with only slight oversimulation for both frequency and persistence. There are fewer outliers in the number of ridge days per year than there were for ridge length, meaning that the models seem to do a better job of simulating ridge frequency than persistency. This is expected, as the use of standardized anomalies when defining ridges constrains the number of days that can be a ridge each spring. There appears to be a very slight decrease in frequency and persistence of future ridges, but there is no quantitative statistical significance as no statistical significance test was applied. A caveat to this study is that only ten CMIP6 models were used, as at the time of research only ten models were available with sufficient data across all three time periods. These models provide a reasonable view of projected changes in ridging, but more models would be ideal to further understand the project at hand.

These results show insubstantial changes in atmospheric ridging in the future. This could mean that the two aforementioned hypothesized causes for atmospheric ridging changes, AA and SST, will change very little and even reduce geopotential height anomalies. However, more research must be done to understand the effects that AA and SST could have on ridges, as well as how climate change will affect AA and SST. Potential future ridging research could focus on multi-decadal moving averages in order to create a more comprehensive understanding of atmospheric ridging. Additional research may add more CMIP6 models, as well as focus closely on dynamics associated with atmospheric ridging.

The findings of this study do not suggest systematic changes in springtime atmospheric ridging frequency or persistence in the Pacific Northwest. However, results are limited in focus with data from only ten CMIP6 models. The results discussed here are inconsistent with discussed changes in SST and AA, but other dynamics may play larger roles in the mechanisms behind atmospheric ridging than currently understood. Additionally, this study was focused on the Pacific Northwest, which does not mean that SST and AA do not affect ridging elsewhere.

While ridging anomalies may decrease in frequency and persistency in the future, the atmosphere will expand, potentially causing ridge-like effects throughout the entire Pacific Northwest regardless of the presence of persistent positive anomalies. Thus, heat-related impacts from ridges will likely be more severe than at present.

This study introduced a ridge detection algorithm based on 500 hPa geopotential height anomalies across a localized area. This approach can be used in other areas directly affected by atmospheric ridging, but must be adapted for the specific area. Future research could focus on reaching a deeper understanding of the future of atmospheric ridging in the Pacific Northwest.

Bibliography

Barnes, E. A., 2013: Revisiting the evidence linking Arctic amplification to extreme weather in midlatitudes. *Geophysical Research Letters*, **40**, 4734–4739, https://doi.org/10.1002/grl.50880.

Bentsen, M., and Coauthors, 2019: NCC NorESM2-MM model output prepared for CMIP6 CMIP historical, Version 20191001. Earth System Grid Federation, accessed 1 October 2019, https://doi.org/10.22033/ESGF/CMIP6.8040.

—— and Coauthors, 2019: NCC NorESM2-MM model output prepared for CMIP6 ScenarioMIP ssp585, Version 20191001. Earth System Grid Federation, accessed 1 October 2019, https://doi.org/10.22033/ESGF/CMIP6.8321.

Bond, N. A., and D. E. Harrison, 2000: The Pacific decadal oscillation, air-sea interaction and central north Pacific winter atmospheric regimes. *Geophysical Research Letters*, **27**, 731–734, https://doi.org/10.1029/1999GL010847.

Brewer, M. C., and C. F. Mass, 2016: Projected Changes in Western U.S. Large-Scale Summer Synoptic Circulations and Variability in CMIP5 Models. *J. Climate*, **29**, 5965–5978, https://doi.org/10.1175/JCLI-D-15-0598.1.

Davini, P., C. Cagnazzo, S. Gualdi, and A. Navarra, 2012: Bidimensional Diagnostics, Variability, and Trends of Northern Hemisphere Blocking. *J. Climate*, **25**, 6496–6509, https://doi.org/10.1175/JCLI-D-12-00032.1.

Danabasoglu, G., 2019: NCAR CESM2-WACCM model output prepared for CMIP6 CMIP historical, Version 20191001. Earth System Grid Federation, accessed 1 October 2019, https://doi.org/10.22033/ESGF/CMIP6.11298.

—— , 2019: NCAR CESM2-WACCM model output prepared for CMIP6 ScenarioMIP ssp585, Version 20191001. Earth System Grid Federation, accessed 1 October 2019, https://doi.org/10.22033/ESGF/CMIP6.10115

Francis, J., and N. Skific, 2015: Evidence linking rapid Arctic warming to mid-latitude weather patterns. *Philos Trans A Math Phys Eng Sci*, **373**, https://doi.org/10.1098/rsta.2014.0170.

—— and S. J. Vavrus, 2012: Evidence linking Arctic amplification to extreme weather in mid-latitudes. *Geophysical Research Letters*, **39**, https://doi.org/10.1029/2012GL051000.

——, N. Skific, and S. J. Vavrus, 2018: North American Weather Regimes Are Becoming More Persistent: Is Arctic Amplification a Factor? *Geophysical Research Letters*, **45**, 11,414-11,422, https://doi.org/10.1029/2018GL080252.

Gao, X., C. A. Schlosser, P. A. O'Gorman, E. Monier, and D. Entekhabi, 2017: Twenty-First-Century Changes in U.S. Regional Heavy Precipitation Frequency Based on Resolved Atmospheric Patterns. *J. Climate*, **30**, 2501–2521, https://doi.org/10.1175/JCLI-D-16-0544.1.

Gelaro, R., and Coauthors, 2017: The Modern-Era Retrospective Analysis for Research and Applications, Version 2 (MERRA-2). *J. Climate,* **30**, 5419–5454, https://doi.org/10.1175/JCLI-D-16-0758.1.

Gibson, P. B., D. E. Waliser, B. Guan, M. J. DeFlorio, F. M. Ralph, and D. L. Swain, 2020: Ridging Associated with Drought across the Western and Southwestern United States: Characteristics, Trends, and Predictability Sources. *J. Climate*, **33**, 2485–2508, https://doi.org/10.1175/JCLI-D-19-0439.1.

Guo, H., and Coauthors, 2018: NOAA-GFDL GFDL-CM4 model output prepared for CMIP6 CMIP historical, Version 20191001. Earth System Grid Federation, accessed 1 October 2019, https://doi.org/10.22033/ESGF/CMIP6.8594.

——, and Coauthors, 2018: NOAA-GFDL GFDL-CM4 model output prepared for CMIP6 ScenarioMIP ssp585, Version 20191001. Earth System Grid Federation, accessed 1 October 2019, https://doi.org/10.22033/ESGF/CMIP6.9268.

Hoskins, B., and T. Woollings, 2015: Persistent Extratropical Regimes and Climate Extremes. *Curr Clim Change Rep*, **1**, 115–124, https://doi.org/10.1007/s40641-015-0020-8.

Jungclaus, J., and Coauthors, 2019: MPI-M MPI-ESM1.2-HR model output prepared for CMIP6 CMIP historical, Version 20191001. Earth System Grid Federation, accessed 1 October 2019, https://doi.org/10.22033/ESGF/CMIP6.6594.

Liu, P., and Coauthors, 2018: Climatology of tracked persistent maxima of 500-hPa geopotential height. *Climate Dynamics; Heidelberg*, **51**, 701–717, http://dx.doi.org.proxy.lib.pdx.edu/10.1007/s00382-017-3950-0.

Loikith, P. C., B. R. Lintner, and A. Sweeney, 2017: Characterizing Large-Scale Meteorological Patterns and Associated Temperature and Precipitation Extremes over the Northwestern United States Using Self-Organizing Maps. *J. Climate*, **30**, 2829–2847, https://doi.org/10.1175/JCLI-D-16-0670.1.

Mundhenk, B. D., E. A. Barnes, E. D. Maloney, and K. M. Nardi, 2016: Modulation of atmospheric rivers near Alaska and the U.S. West Coast by northeast Pacific height anomalies. *Journal of Geophysical Research: Atmospheres*, **121**, 12,751-12,765, https://doi.org/10.1002/2016JD025350.

Newman, M., and Coauthors, 2016: The Pacific Decadal Oscillation, Revisited. *J. Climate*, **29**, 4399–4427, https://doi.org/10.1175/JCLI-D-15-0508.1.

Parsons, S., J. A. Renwick, and A. J. McDonald, 2016: An Assessment of Future Southern Hemisphere Blocking Using CMIP5 Projections from Four GCMs. *J. Climate*, **29**, 7599–7611, https://doi.org/10.1175/JCLI-D-15-0754.1.

Peng, P., A. Kumar, M. Chen, Z.-Z. Hu, and B. Jha, 2019: Was the North American extreme climate in winter 2013/14 a SST forced response? *Clim Dyn*, **52**, 3099–3110, https://doi.org/10.1007/s00382-018-4314-0.

Renwick, J. A., 2005: Persistent Positive Anomalies in the Southern Hemisphere Circulation. *Mon. Wea. Rev.*, **133**, 977–988, https://doi.org/10.1175/MWR2900.1.

Röthlisberger, M., S. Pfahl, and O. Martius, 2016: Regional-scale jet waviness modulates the occurrence of midlatitude weather extremes. *Geophysical Research Letters*, **43**, 10,989-10,997, https://doi.org/10.1002/2016GL070944.

Schupfner, M., and Coauthors, 2019: DKRZ MPI-ESM1.2-HR model output prepared for CMIP6 ScenarioMIP ssp585, Version 20191001. Earth System Grid Federation, accessed 1 October 2019, https://doi.org/10.22033/ESGF/CMIP6.4403.

Screen, J. A., and I. Simmonds, 2013: Exploring links between Arctic amplification and mid-latitude weather. *Geophysical Research Letters*, **40**, 959–964, https://doi.org/10.1002/grl.50174.

Seager, R., and N. Henderson, 2016: On the Role of Tropical Ocean Forcing of the Persistent North American West Coast Ridge of Winter 2013/14. *J. Climate*, **29**, 8027–8049, https://doi.org/10.1175/JCLI-D-16-0145.1.

——, M. Hoerling, S. Schubert, H. Wang, B. Lyon, A. Kumar, J. Nakamura, and N. Henderson, 2015: Causes of the 2011–14 California Drought. *J. Climate*, **28**, 6997–7024, https://doi.org/10.1175/JCLI-D-14-00860.1.

Seland, Ø., and Coauthors, 2019: NCC NorESM2-LM model output prepared for CMIP6 CMIP historical, Version 20191001. Earth System Grid Federation, accessed 1 October 2019, https://doi.org/10.22033/ESGF/CMIP6.8036.

——, and Coauthors, 2019: NCC NorESM2-LM model output prepared for CMIP6 ScenarioMIP ssp585, Version 20191001. Earth System Grid Federation, accessed 1 October 2019, https://doi.org/10.22033/ESGF/CMIP6.8319.
Shiogama, H., and Coauthors, 2019: MIROC MIROC6 model output prepared for CMIP6 ScenarioMIP ssp585, Version 20191001. Earth System Grid Federation, accessed 1 October 2019, https://doi.org/10.22033/ESGF/CMIP6.5771.
Swain, D. L., 2015: A tale of two California droughts: Lessons amidst record warmth and dryness in a region of complex physical and human geography. *Geophysical Research Letters*, **42**, 9999-10,003, https://doi.org/10.1002/2015GL066628.
——, D. Singh, D. E. Horton, J. S. Mankin, T. C. Ballard, and N. S. Diffenbaugh, 2017: Remote Linkages to Anomalous Winter Atmospheric Ridging Over the Northeastern Pacific. *Journal of Geophysical Research: Atmospheres*, **122**, 12,194-12,209, https://doi.org/10.1002/2017JD026575.
Swart, N., and Coauthors, 2019: CCCma CanESM5 model output prepared for CMIP6 CMIP historical, Version 20191001. Earth System Grid Federation, accessed 1 October 2019, https://doi.org/10.22033/ESGF/CMIP6.3610.
——, and Coauthors, 2019: CCCma CanESM5 model output prepared for CMIP6 ScenarioMIP ssp585, Version 20191001. Earth System Grid Federation, accessed 1 October 2019, https://doi.org/10.22033/ESGF/CMIP6.3696.
Tatebe, H., and Watanabe, M., 2018: MIROC MIROC6 model output prepared for CMIP6 CMIP historical, Version 20191001. Earth System Grid Federation, accessed 1 October 2019, https://doi.org/10.22033/ESGF/CMIP6.5603.
Teng, H., and G. Branstator, 2017: Causes of Extreme Ridges That Induce California Droughts. *J. Climate*, **30**, 1477–1492, https://doi.org/10.1175/JCLI-D-16-0524.1.
USDA Natural Resources Conservation Service, 2019: Blazed Alder Historical Daily Precipitation. SNOwpack Telemetry Network (SNOTEL), accessed 1 May 2019, https://data.nal.usda.gov/dataset/snowpack-telemetry-network-snotel.
Volodin, E., and Coauthors, 2019: INM INM-CM5-0 model output prepared for CMIP6 CMIP historical, Version 20191001. Earth System Grid Federation, accessed 1 October 2019, https://doi.org/10.22033/ESGF/CMIP6.5070.
——, and Coauthors, 2019: INM INM-CM5-0 model output prepared for CMIP6 ScenarioMIP ssp585, Version 20191001. Earth System Grid Federation, accessed 1 October 2019, https://doi.org/10.22033/ESGF/CMIP6.12338.
Wang, S.-Y., L. Hipps, R. R. Gillies, and J.-H. Yoon, 2014: Probable causes of the abnormal ridge accompanying the 2013-2014 California drought: ENSO precursor and anthropogenic warming footprint: DIAGNOSING CALIFORNIA DROUGHT 2013-14. *Geophys. Res. Lett.*, **41**, 3220–3226, https://doi.org/10.1002/2014GL059748.
Woollings, T., and Coauthors, 2018: Blocking and its Response to Climate Change. *Curr Clim Change Rep*, **4**, 287–300, https://doi.org/10.1007/s40641-018-0108-z.
Wu, Tongwen and Coauthors, 2019: BCC BCC-CSM2MR model output prepared for CMIP6 CMIP historical, Version 20191001. Earth System Grid Federation, accessed 1 October 2019, https://doi.org/10.22033/ESGF/CMIP6.2948.
Xin, X., and Coauthors, 2019: BCC BCC-CSM2MR model output prepared for CMIP6 ScenarioMIP ssp585, Version 20191001. Earth System Grid Federation, accessed 1 October 2019, https://doi.org/10.22033/ESGF/CMIP6.3050.

Yukimoto, S., and Coauthors, 2019: MRI MRI-ESM2.0 model output prepared for CMIP6 ScenarioMIP ssp585, Version 20191001. Earth System Grid Federation, accessed 1 October 2019, https://doi.org/10.22033/ESGF/CMIP6.6929.

——, and Coauthors, 2019: MRI MRI-ESM2.0 model output prepared for CMIP6 CMIP historical, Version 20191001. Earth System Grid Federation, accessed 1 October 2019, https://doi.org/10.22033/ESGF/CMIP6.6842